ISTITUTO NAZIONALE DI GEOFISICA E VULCANOLOGIA

Site characterization report at the seismic station IT.SARM – Sarmato (PC)

Report di caratterizzazione di sito presso la stazione sismica IT.SARM – Sarmato (PC)

Working Group **Geology:** Paolo MANGANELLO, Sara LOVATI **Geophysics**: Rodolfo PUGLIA, Giulio BRUNELLI, Alessio LORENZETTI, Sara LOVATI, Paolo MANGANELLO, Marco MASSA	Date: December 2021
Subject: **Final report illustrating the site characterization for seismic station IT.SARM**	

Convenzione DPC-INGV 2019-21, All. B2- WP1, Task 2: "Caratterizzazione siti accelerometrici" (Coord.: G. Cultrera, F. Pacor)
Cite as: Working group INGV "Agreement DPC-INGV 2019-21, All. B2- WP1, Task 2" (2021). Site characterization report at the seismic station *IT.SARM – Sarmato (PC).* http://hdl.handle.net/2122/15040

INDEX

INTRODUCTION

In this report we present the geological setting and the geophysical measurements and results obtained in the framework of the 2019-2021 agreement between INGV and DPC, called *Allegato B2: Obiettivo 1 - TASK 2: Caratterizzazione siti accelerometrici (Responsabili: G. Cultrera, F. Pacor)* for the site characterization of station IT.SARM (Sarmato).

Location and coordinates are reported in Table 1.

Table 1

CODE	NAME	LAT [°]	LON [°]	ELEVATION [m]
IT.SARM	Sarmato (PC)	45.0544 *	9.4900 *	75 **
ADDRESS	Via Emilia, Cascina Mammalucca, 29010 Sarmato (PC), Italy			

* Coordinates from ITACA (Nov. 2021) ** Elevation from CTR 5k Regione Emilia-Romagna

A. Geological setting

A1. TOPOGRAPHIC AND GEOLOGICAL INFORMATION

Topographic information related to the site are reported in Table 2. Table 3 summarizes all available geological maps from literature for geological analyses.

Table 2

Topography	Description	Topography Class	Morphology Class
	Flat surfaces, isolated slopes and reliefs with slope i ≤ 15°	T1	Plain (P)

Table 3

Geological map	Source	Scale
IT.SARM	Geological Map of Italy, sheet 60 (Piacenza)	1:100.000
IT.SARM	Geologic Technical Map of Sarmato Municipality - Seismic Microzonation	1:10.000

In Table 4 Geological, Lithological and Lithotechnical Units (according to Seismic Microzonation classification; Technical Commission SM, 2015) are described and are concerned to maps of following chapters. The term "original" means the result comes from a preexisting cartography (Table 3); the term "deduced" means the result comes from an interpretation of a preexisting cartography according to the nomenclature of corresponding cartography.

Table 4

GEOLOGICAL UNITS		**LITHOLOGICAL UNITS**		**LITHOTECHNICAL UNITS**	
Geological Map of Italy 1:100.000, sheet 60 (Piacenza) *original*		Amanti *et al.* (2008) *deduced*		(MZS) *original*	
code	**description**	**code**	**description**	**code**	**description**
f^R	Fluvial Riss	B2	Sandy-silty soils	CLtf	Sandy-silty clays

A2. GEOLOGICAL MAP

In Figure 1 Geological Map is reported in a 1 *km* × 1 *km* square around the station.

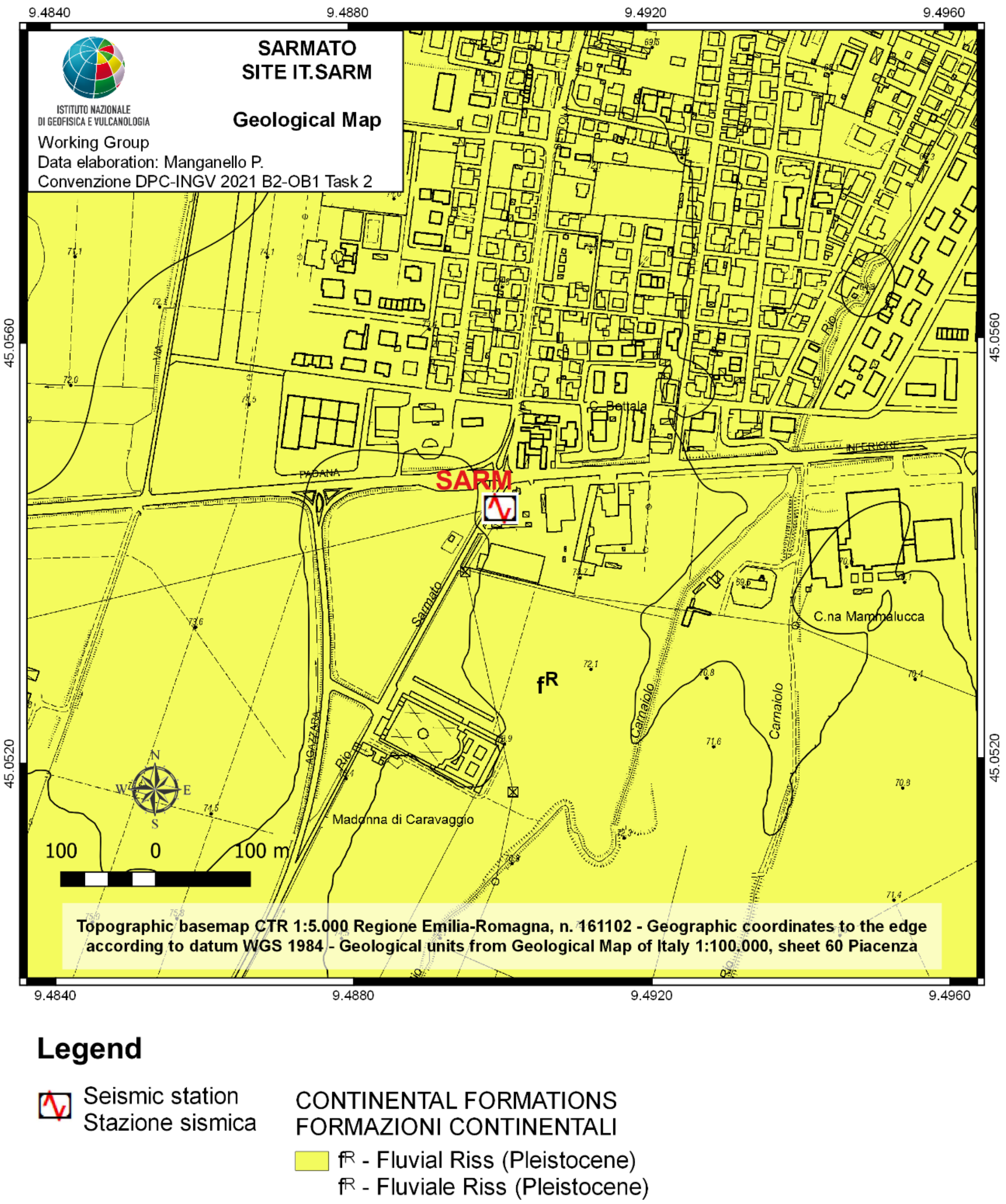

Figure 1: Geological map of seismic station IT.SARM. Scale 1:5.000. Geological units come from Geological Map of Italy 1:100.000, sheet 60 Piacenza.

A3. LITHOLOGICAL MAP

In Figure 2 Lithological Map is reported in a 1 *km* × 1 *km* square around the station.

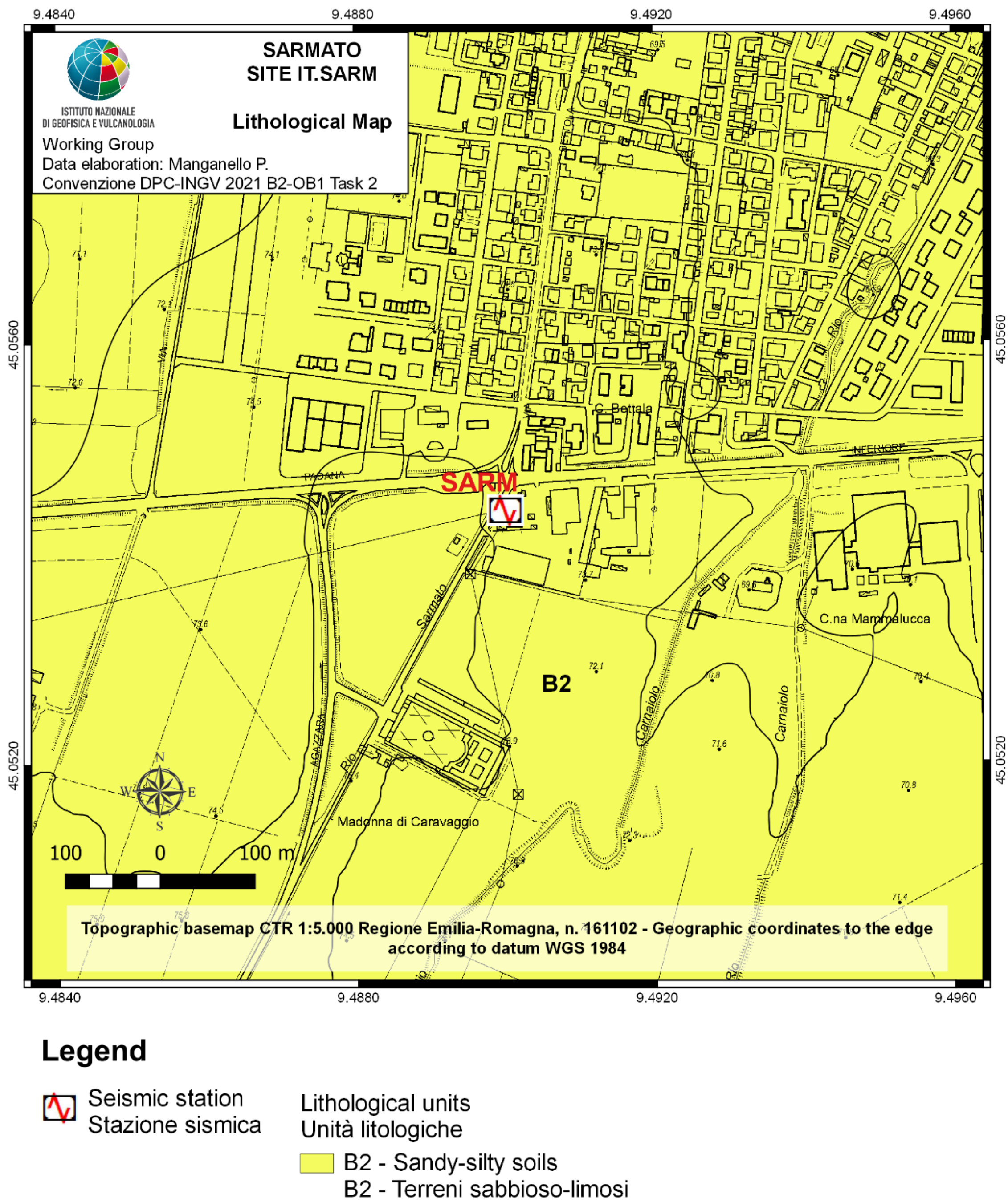

Figure 2: Lithological map of the seismic station IT.SARM. Scale 1:5.000. The codes of the lithological units are assigned according to the nomenclature of the Lithological map of Italy ISPRA 1:100.000 (Amanti *et al.*, 2008).

A4. LITHOTECHNICAL MAP

In Figure 3 Lithotechnical Map is reported in a 1 *km* × 1 *km* square around the station.

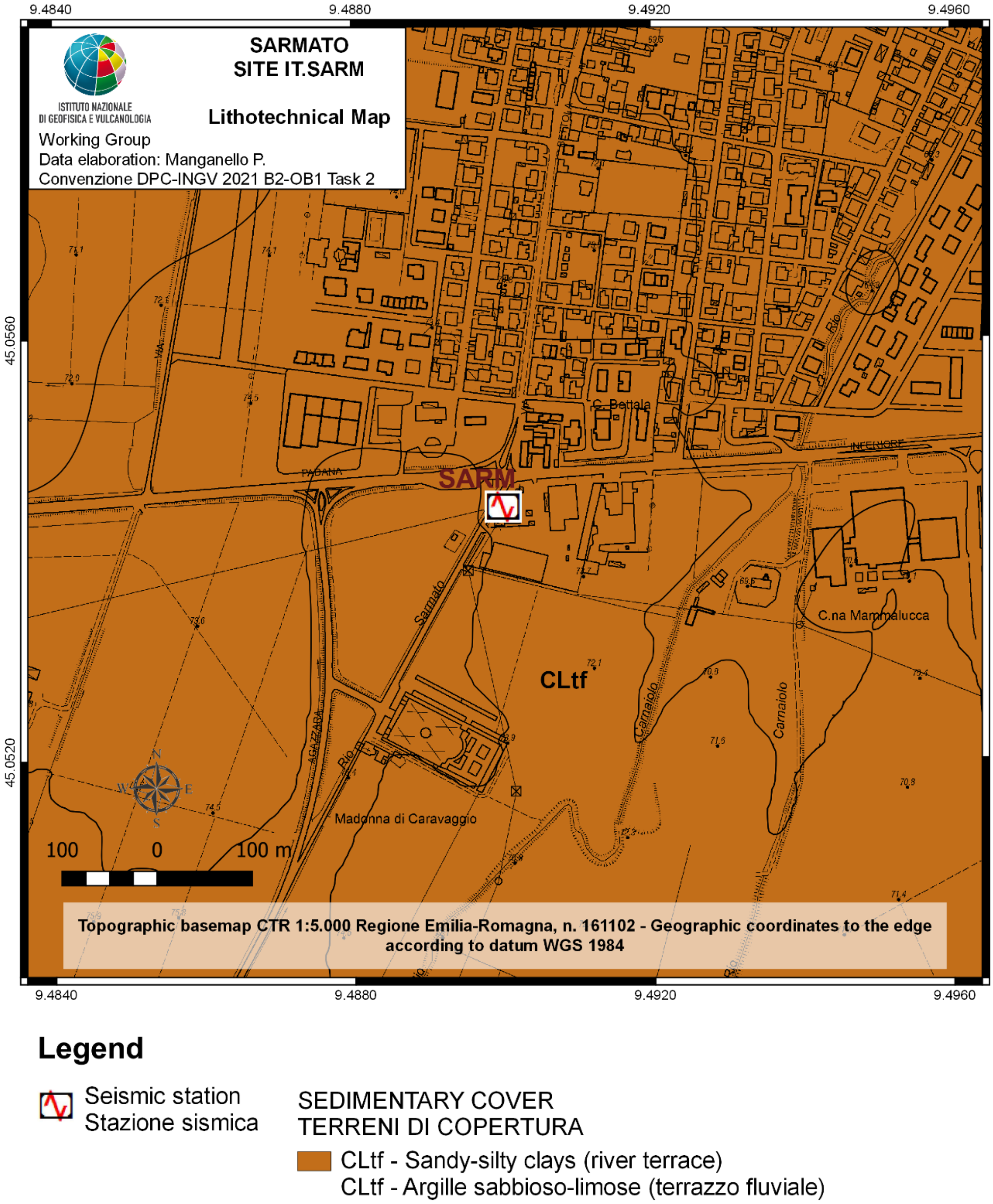

Figure 3: Lithotechnical map of the seismic station IT.SARM. Scale 1:5.000. The lithotechnical units are assigned according to the nomenclature of Seismic Microzonation (Technical Commission SM, 2015).

A5. SURVEY MAP

Figure 4 shows the Survey Map reporting both previous investigations and geophysical surveys conducted by INGV Working Group.

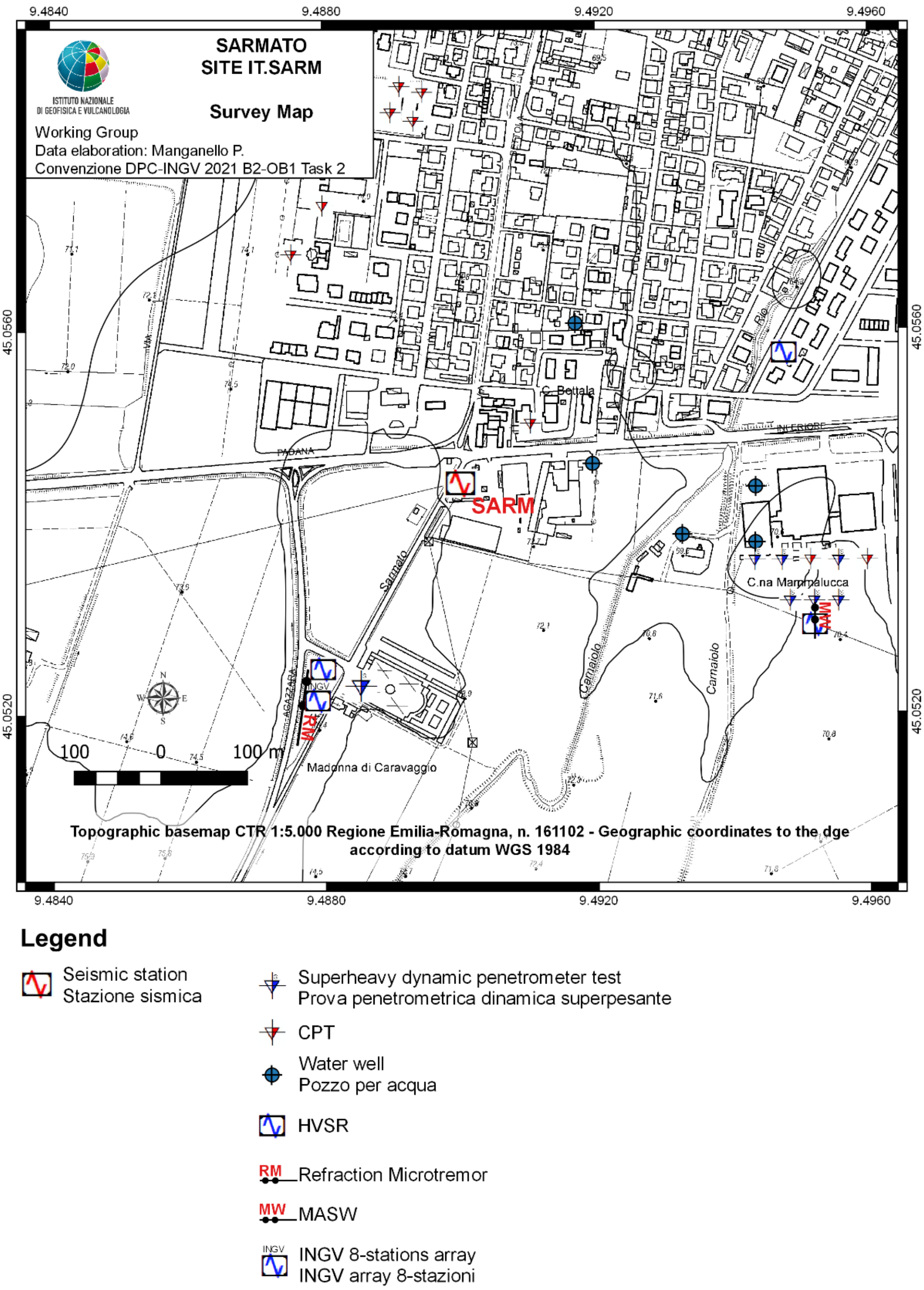

Figure 4: Map of the surveys in the surroundings of the station IT.SARM. Scale 1:5.000.

A6. GEOLOGICAL MODEL

6.1 General description

The seismic station IT.SARM is installed in the Sarmato municipality, which is located in the north-western sector of Piacenza Province. The Sarmato municipality is delimited to the North by the right bank of Po river.

The geological setting of the studied area is related with the evolution of the Po Plain sedimentary basin, which represents the foreland basin of the Northern Apennines and the retroforeland basin of the Alps. The Po Plain originates since the Late Cretaceous, as a consequence of the thrusting of the south verging Southern Alps and the north-northeast verging Northern Apennines belts, that loaded and bended the continental crust giving rise to a foreland basin characterized by a thick synorogenic clastic sequence and complex buried tectonic structures. In the Pliocene until the Lower Pleistocene the sea yet covered the area of the current Po Plain forming a marine gulf between the Alps and the Apennines affected by a quite deep sedimentation controlled by subsidence. Plio-Pleistocene sea sediments, generally consisting of clays, silts and sands, have very high thickness, in some areas of the orders of some kilometers. Successively the transition from Marine Quaternary to Continental Quaternary took place with the sedimentation of fluvial sediments, controlled by tectonic processes and climate changes, until the deposition of exclusively continental Holocene sediments, with a gradually filling of the sedimentary basin from West to East (Doglioni, 1993; Carminati and Doglioni, 2012; Fantoni and Franciosi, 2010).

The territory of Sarmato municipality is characterized by the presence of Pleistocene-Holocene alluvial deposits of the Upper Emiliano-Romagnolo Synthem, consisting in clays, silts with sandy intercalations and gravelly sands. The southern-central area of the Sarmato municipality is interested by the deposition of alluvial sediments of Apenninic origin, while the northern area is characterized by depositional and erosional activities of the Po river (Comune di Sarmato, 2020).

6.2 Geological section

The stratigraphic information in the surroundings of IT.SARM seismic station are represented by five water wells. The other executed surveys consist in Cone Penetrometer Tests (CPT), Superheavy Dynamic Penetrometer Tests, single station noise measurements (HVSR), MASW and Refraction Microtremor surveys.

The WSW-ENE oriented geological section is reported and highlights the geological and structural setting of IT.SARM site. The trace with the location of the section is reported as a black line in the geological map (Fig. 5 upper left).

6.3 Subsoil model

The geological description reported from the surface to the bottom is described in the following part. A subsoil model is built up to a depth of 40 *m* on the basis of geological information (Fig. 5 bottom). The stratigraphic succession is characterized by the alluvial deposits of the Fluvial Riss continental formation (Pleistocene), represented by a shallow clayey layer with a thickness of about 10-15 *m* and a deeper gravelly-sandy layer.

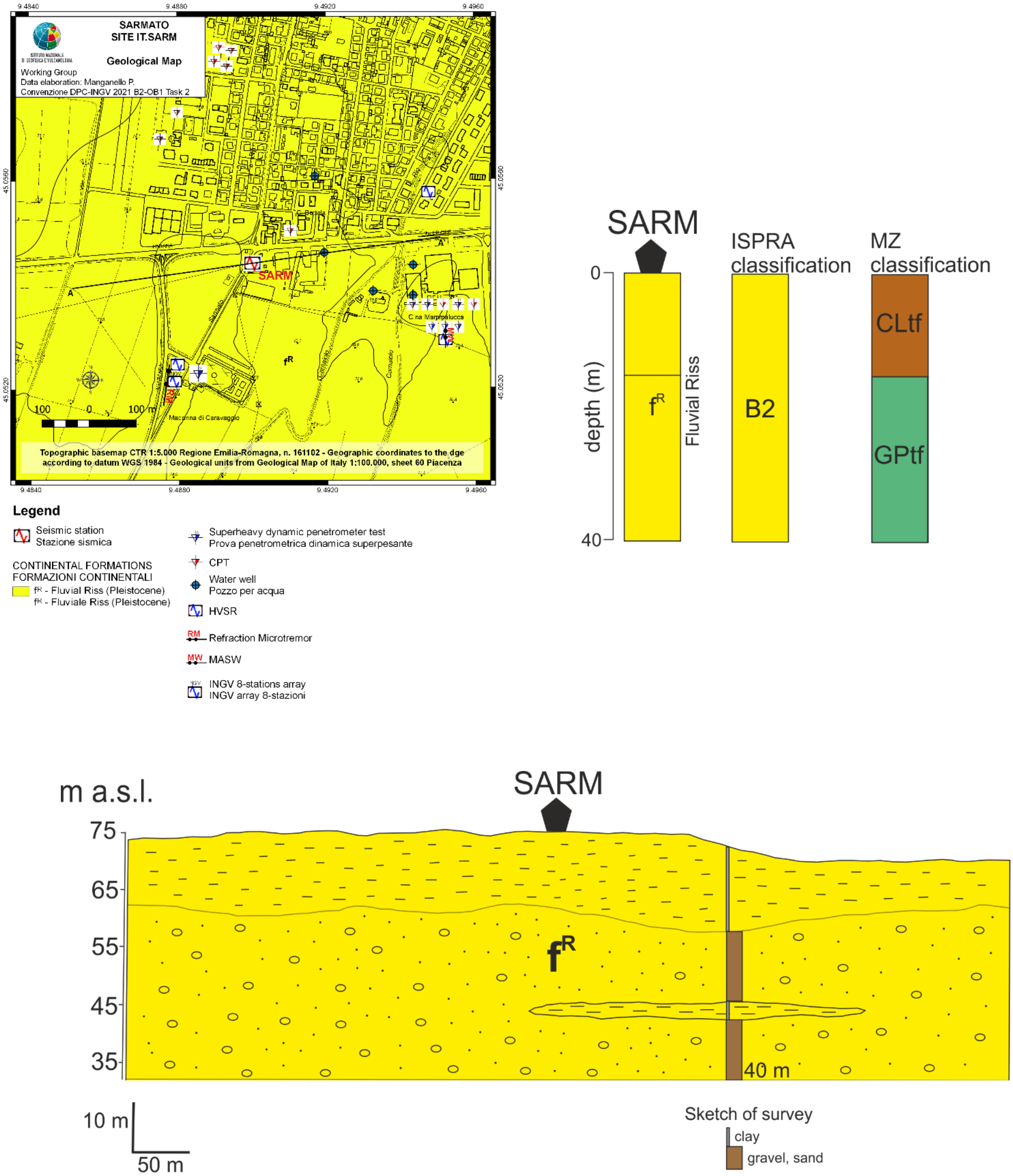

Figure 5: Upper left: Geological map of the study area where is installed IT.SARM seismic station. Upper right: Geological section. Bottom: Subsoil model for the site.

B. V_S profile

B1. GEOPHYSICAL INVESTIGATIONS

Geophysical measurements executed nearby the station SARM of the network IT (PCM-DPC, 1972) consist in ambient-vibration measurements in both single-station and 2D array configuration (Figure 6) that provide results in terms of resonance frequency of the soil deposits and in terms of dispersion curves of surface waves. These curves are inverted to obtain a shear-wave velocity (V_S) profile that, together with the geological study at section A, is suitable for assigning the soil class according to the current Italian seismic code (NTC18) and Eurocode (EC8). Figure 7 shows the location of the station IT.SARM (Latitude 45.0544, Longitude 9.4900 WGS84) installed at Sarmato (PC).

Seismic noise is acquired using 8 Reftek-130 24-bits recording systems equipped with short-period Lennartz LE-3D/5s sensors and GPS timing (Figure 7). The sampling rate is fixed to 200 *Hz*, while the gain is set as “high”. Ambient noise recordings have a minimum duration of 1 hour. The array geometry (Figure 8) is chosen in order to have a good coverage of both azimuths and inter-station distances, the latter between the minimum (less than 10 *m*) and the maximum (about 30 *m*). These ranges allow the analysis of a range of wavelengths that guarantee sufficient shallow resolution (Okada, 2003) in order to estimate the $V_{S,30}$ and the site-class according to current building codes (i.e. NTC18 and EC8).

Figure 6: Map of the geophysical measurements performed at the IT.SARM site. The yellow place-markers indicate the geometry used for 2D array in passive configuration. The red triangle indicates the IT.SARM accelerometric station (image from Google Earth http://www.earth.google.com).

Figure 7: Left: ENEL cabin where the IT.SARM accelerometric station is installed in Sarmato (PC). Upper right: single station ambient noise measurement. Bottom right: 2D passive ambient noise array installed close to the IT.SARM station.

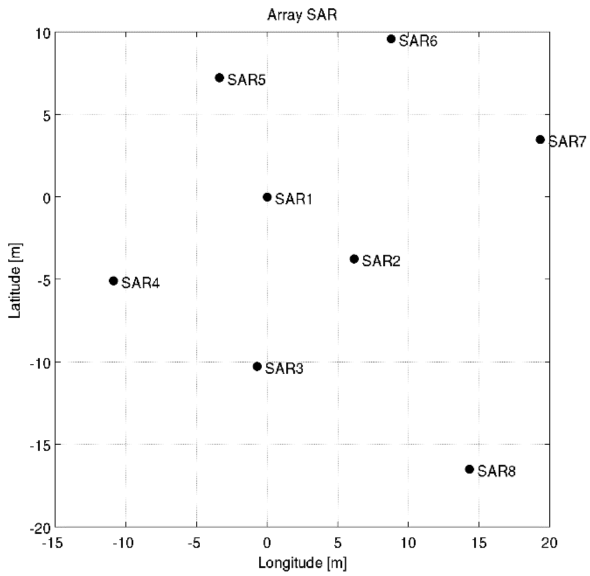

Figure 8: Array geometry.

The first step of the analysis consists in a visual inspection of the recordings at each station of the array. In particular, in order to identify malfunctioning and to select signal windows suitable for the surface wave analysis, the quality of the recording is evaluated analyzing the signal stationarity in the time domain, the relevant unfiltered Fourier spectra, and the H/V variation over time. Figures 9 and 10 provide graphical results about station SAR3.

It is common practice during surface wave investigation to verify the reliability of the one-dimensional site structure assumption (Aki, 1957; Okada, 2003). For this reason, we estimated the HVSR at each station of the array and the stability of HVSR among the array stations has been verified. Figure 11 depicts the HVSR assumed as representative for the array.

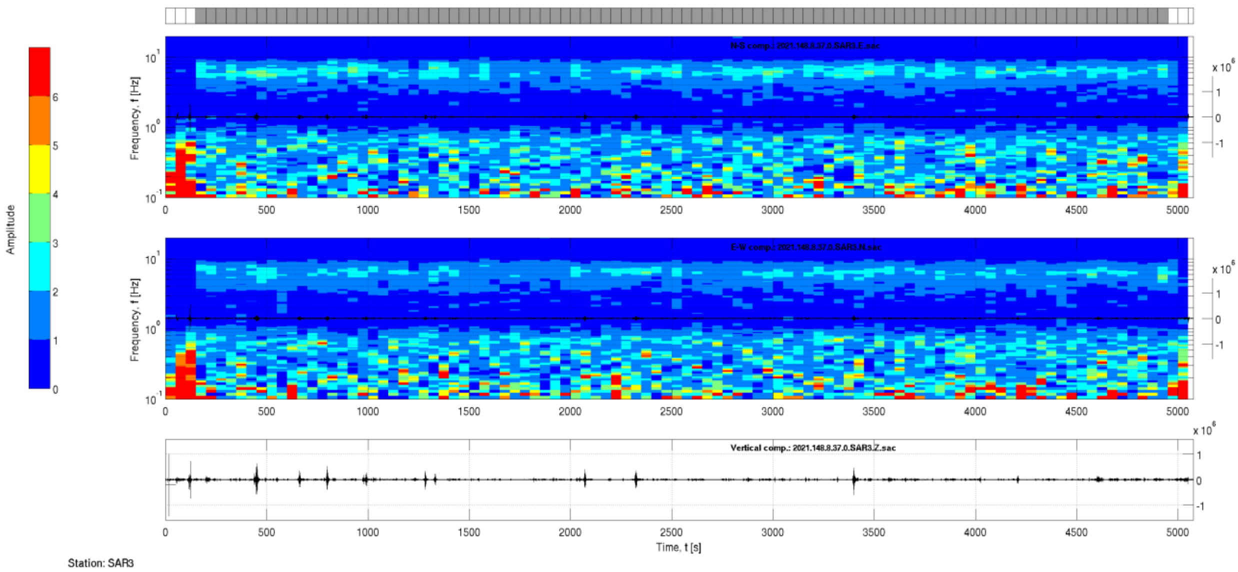

Figure 9: HVSR versus time (top and central panel for the NS and EW component, respectively) and corresponding time-histories.

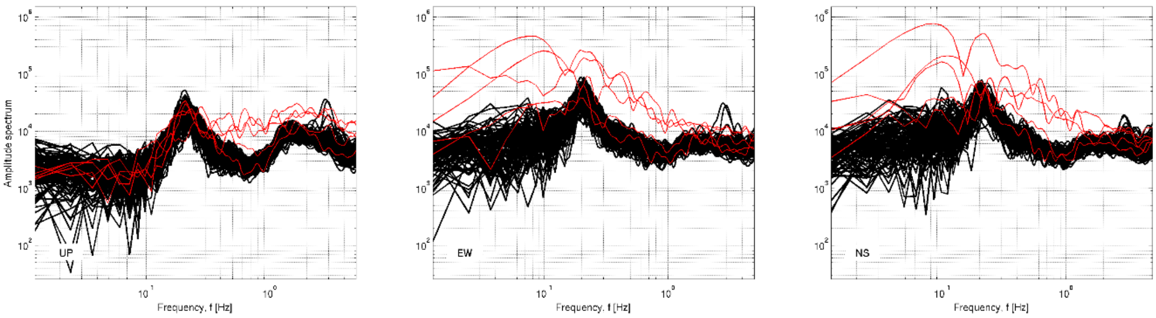

Figure 10: Fourier spectra for each noise window (left: Vertical, center: EW, right: NS). Red spectra are excluded from HVSR analysis.

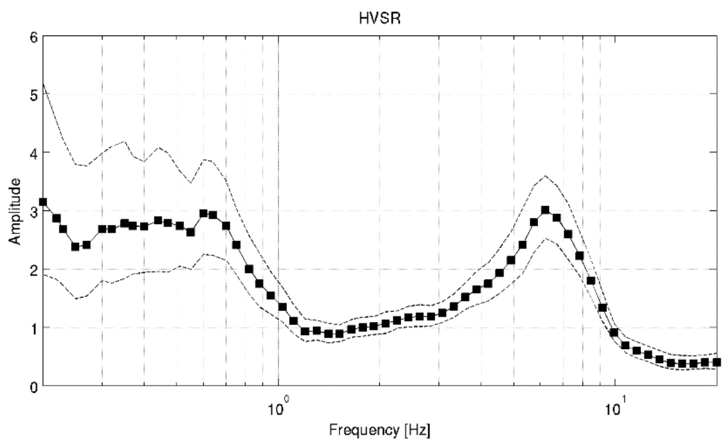

Figure 11: HVSR representative for the array. Dashed lines represent +/- one standard deviation.

The Rayleigh-wave dispersion curve is estimated by analyzing the vertical component of the recorded seismic noise. In particular, the Extended Spatial Auto-Correlation (ESAC; Ohori *et al.*, 2002; Okada, 2003) and the frequency-wavenumber (F-K; Lacoss *et al.*, 1969; Capon, 1969) methods are adopted. Further details about the combined use of ESAC and F-K approaches can be found in Parolai *et al.* (2006).

Both analyses use 50 synchronized signal windows of 60 *s* each, extracted from recordings within the UTC date-time interval 2021-05-28 08:55:00 – 2021-05-28T09:45:00, avoiding time periods affected by local disturbance.

The ESAC Rayleigh-wave dispersion curve is obtained by minimizing the root-mean-square (RMS) of the differences between experimental and theoretical Bessel functions (Figure 12). Values differing by more than two standard deviations from those estimated by the best fitting functions are automatically discarded (red circles in Figure 12) and the procedure is repeated iteratively. For this data set, data are also discarded whenever the inter-station distance is 2 times longer than the relevant wavelength. Figure 13 shows the Rayleigh-wave dispersion curve estimated using the ESAC approach.

The F-K analysis allows checking on the noise source distribution. One of the basic assumptions for the application of the ESAC method is indeed that the seismic noise wavefield is nearly isotropic. Figures 14 and 15 show results of the F-K analysis in terms of power density function for several frequencies using the Maximum Likelihood Method (MLM) and the Beam-Forming (BF) respectively. Figure 16 shows the good agreement above 11 *Hz* between the Rayleigh wave dispersion curves estimated by both ESAC and F-K approaches. As expected, due to the array geometry, below this threshold the F-K analysis provides larger phase velocities.

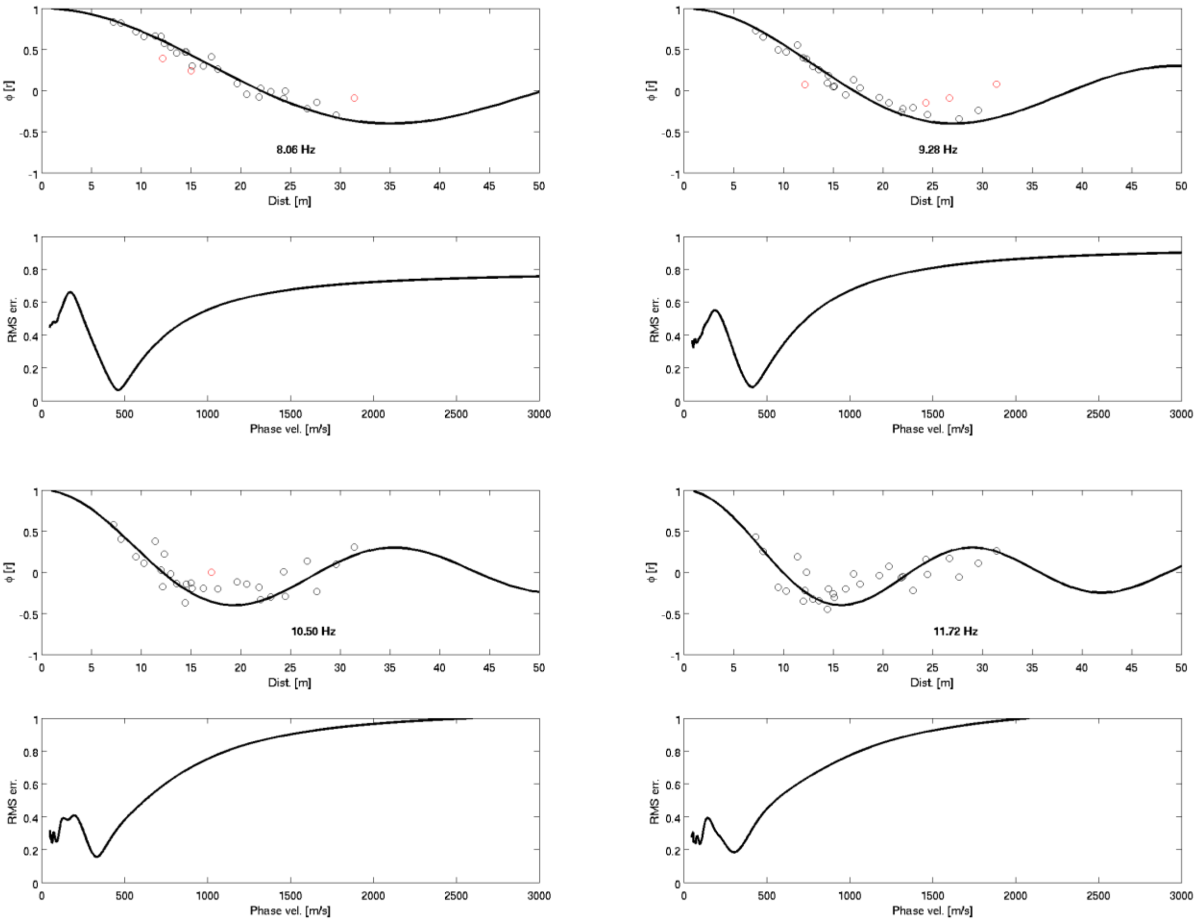

Figure 12: Experimental space-correlation function values versus distance (circles) for different frequencies. The red circles indicate values that are discarded. The black lines depict the estimated space-correlation function values for the phase velocity that furnishes the best fit to the data. The bottom panels show the relevant root-mean-square errors (RMS) versus phase velocity tested.

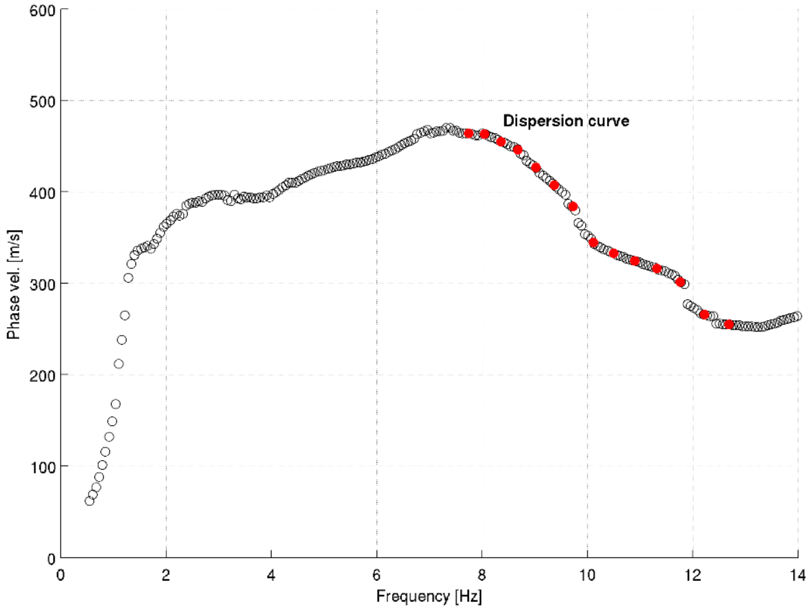

Figure 13: Rayleigh-wave dispersion curve from ESAC. Red-filled circles represent values potentially used for inversions.

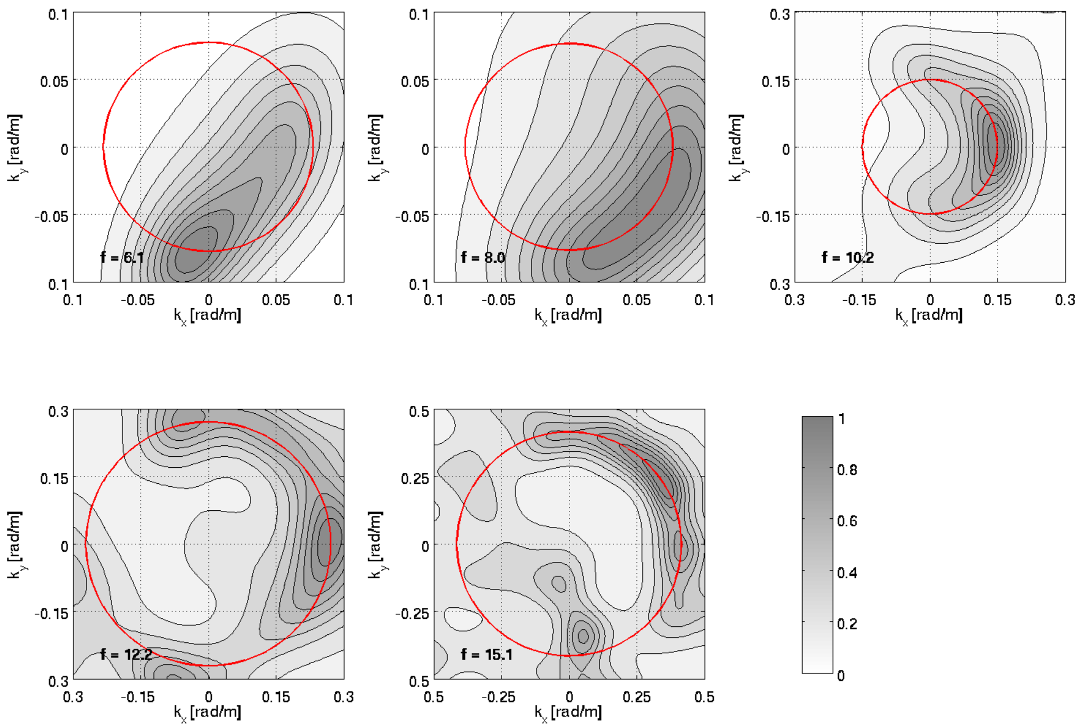

Figure 14: F-K power density function (Maximum-Likelihood Method) at selected frequencies.

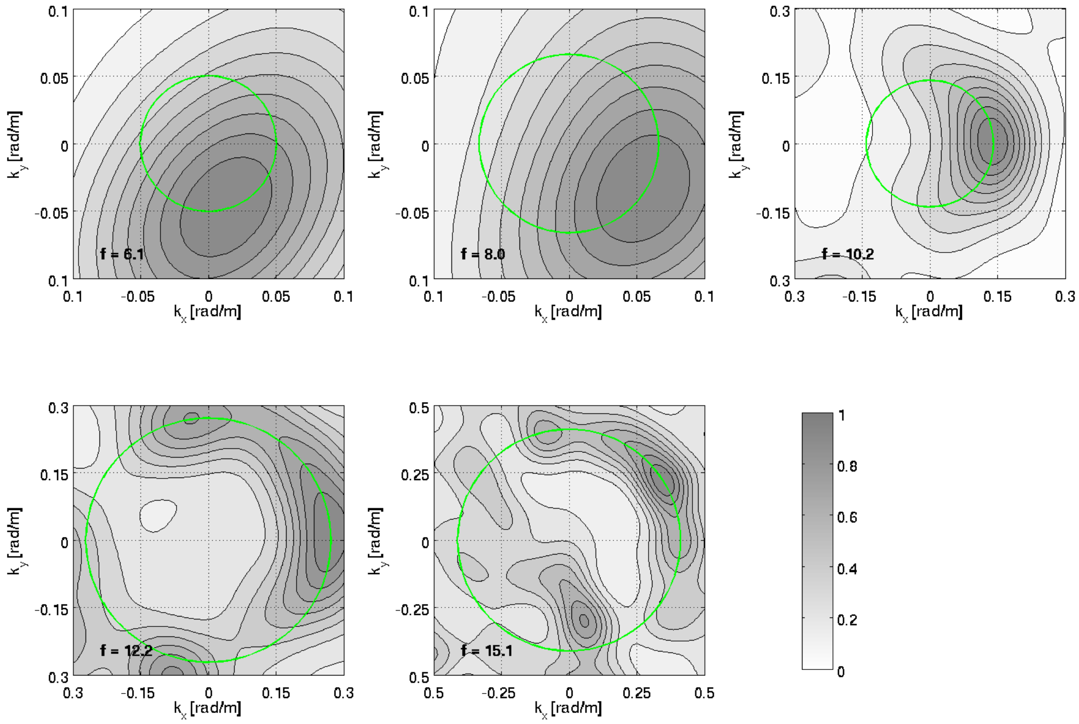

Figure 15: F-K power density function (Beam-Forming) at selected frequencies.

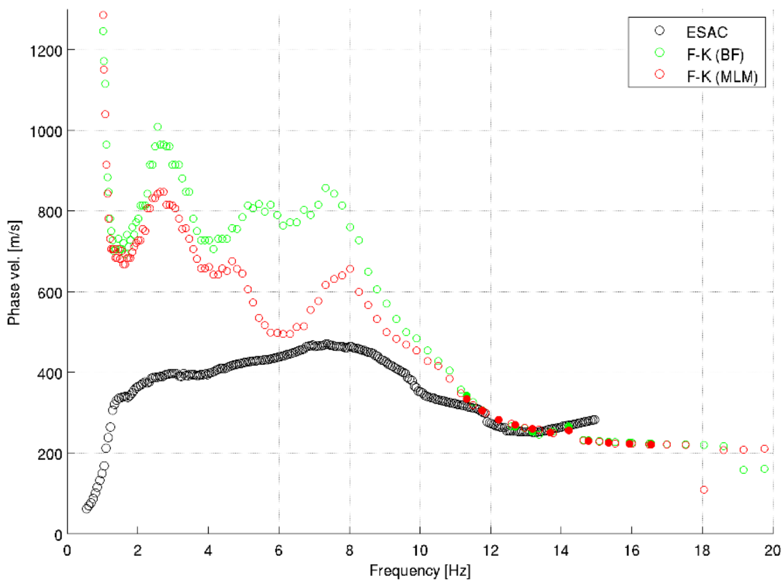

Figure 16: Comparison of experimental phase velocity estimated by the ESAC and the F-K (for both Beam-Forming and Maximum-Likelihood Method) methods. Filled circles represent values potentially used for inversions.

B2. SEISMIC VELOCITY MODEL

The non-linear inversions are performed using the software *joinv6* (Parolai *et al.*, 2005; Giustiniani *et al.*, 2020), which adopt a genetic algorithm (Yamanaka and Ishida, 1996). The forward modelling of Rayleigh wave phase velocities and HVSR curves is performed under the assumption of a vertically heterogeneous 1D Earth model using the modified Thomson-Haskell method proposed by Wang (1999) and following the suggestions of Arai and Tokimatsu (2004) and Tokimatsu *et al.* (1992). The modelling is not restricted to the fundamental mode, preserving the possibility that higher modes participate in simulating the observed dispersion and HVSR curves.

The experimental dispersion curve used as input for inversions is the one estimated from the ESAC analysis in the frequency interval 8-12 *Hz*, in combination with the one from F-K in the interval 12-16 *Hz*. The experimental HVSR is used between about 2 and 10 *Hz*. In the left panel of Figure 17 tested models are shown in different colors according to their cost value: the more reliable model (minimum cost) is in white, the models lying inside the 10% range of the minimum cost are in black and the other tested models are shown in grey. In the right-central and right-bottom panels of Figure 17 agreement between experimental and theoretical (grey and open circles, respectively) Rayleigh-wave dispersion curves and HVSR are shown. The agreement is good and, considering the wavelengths related to the dispersion curve frequency range, the V_S profile between about 5-35 *m* is very well constrained. Table 5 reports the minimum-cost shear-wave velocity model.

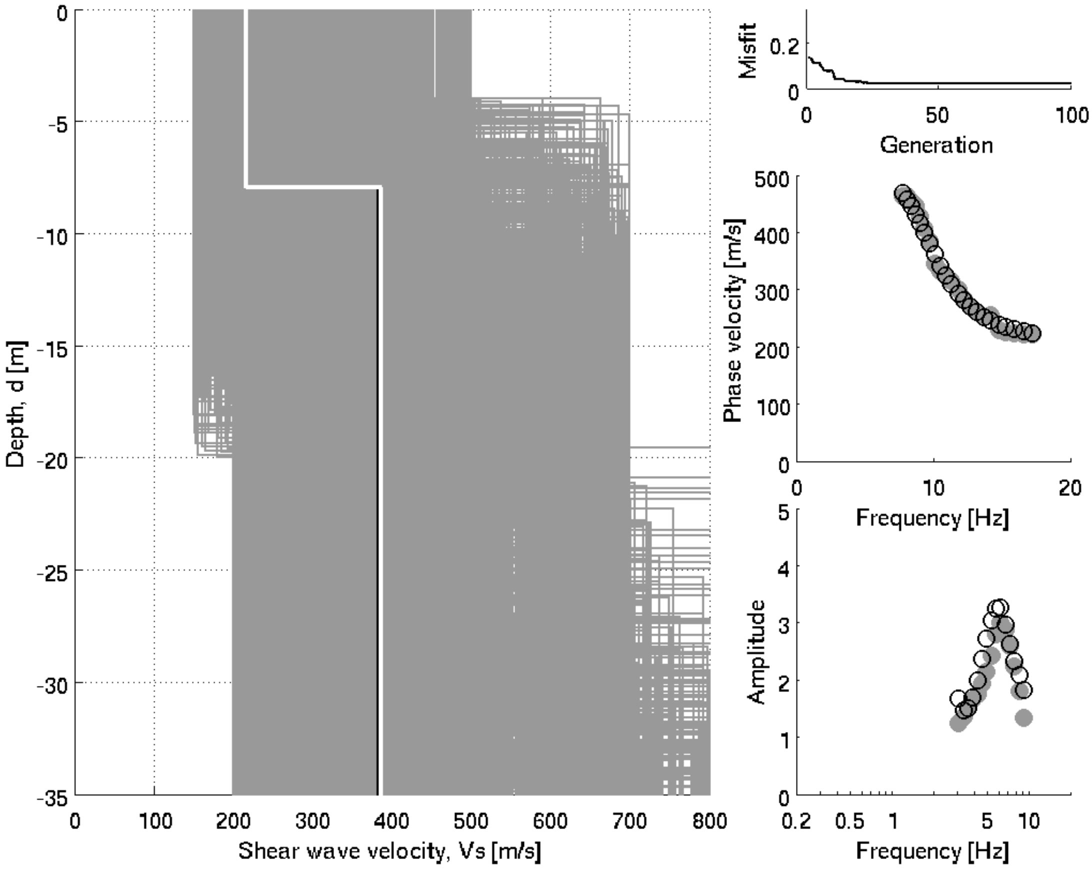

Figure 17: Shear-wave velocity models modeled during the inversion procedure (left panel): tested models (grey lines), the minimum cost model (white line) and models lying inside the minimum cost + 10% range (black lines); the generation values versus misfit (right-upper panel); the fitting of experimental data (grey circles) and empirical values relative to the minimum cost model (white circles) relevant to the dispersion curve (right-central panel) and to HVSR (right-bottom panel).

Table 5: Best-fit shear-wave velocity model

From [*m*]	To [*m*]	Thickness [*m*]	V_S [*m/s*]
0	7.9	7.9	216
7.9	-	-	386

B3. CONCLUSIONS

As evinced from results of geophysical investigations carried out by INGV Working Group, we can attribute to the shallow clayey layer of Fluvial Riss Formation V_S values of 216 m/s and to the deeper sandy-gravelly layer of Fluvial Riss Formation V_S values of 386 m/s, compatible with EC8 class assigned at the site according to geological evidences.
According to the current Italian seismic code (NTC18), if the bedrock (V_S > 800 m/s) is more than 30 m in depth, the equivalent velocity ($V_{S,eq}$) is equal to the $V_{S,30}$. From Figure 17, the velocity of 800 m/s is reached for an unknown depth, well below the depth of 30 m.
Therefore, in this case, both $V_{S,eq}$ and $V_{S,30}$ are equal to 320 m/s. Of consequence, IT.SARM site is classified in the soil category C, for both the NTC18 and EC8 seismic codes (Table 6).

Table 6: $V_{S,eq}$,$V_{S,30}$ and soil classes

$V_{S,eq} = V_{S,30}$ [m/s]	Soil class (NTC18)	Soil class (EC8)
320	C	C

ACKNOWLEDGEMENTS

Authors wish to thank Stefano Parolai, Paolo Bernardi and Ilaria Dreossi (Istituto Nazionale di Oceanografia e di Geofisica Sperimentale – OGS), for providing us the software "joinv6", which has been adopted as inversion procedure to estimate the shear-wave velocity model, and for the precious guide in its usage.

REFERENCES

Aki K. (1957). "Space and time spectra of stationary stochastic waves, with special reference to microtremors", Bulletin of the Earthquake Research Institute, 35, pp. 415–456.

Amanti M., Battaglini L., Campo V., Cipolloni C., Congi M. P., Conte G., Delogu D., Ventura R., Zonetti C. (2008). "The Lithological map of Italy at 1:100.000 scale: An example of re-use of an existing paper geological map", 33rd International Geological Conference, IEI02310L – 6-14th August, Oslo (Norway).

Arai H. and Tokimatsu K. (2004). "S-wave velocity profiling by inversion of microtremor H/V spectrum", Bulletin of the Seismological Society of America, 94, pp. 53–63.

Capon J. (1969). "High-resolution frequency-wavenumber spectrum analysis", Proceedings of the IEEE, 57, pp. 1408–1418.

Carminati E., Doglioni C. (2012). "Alps vs. Apennines: The paradigm of a tectonically asymmetric Earth", Earth-Science Reviews, 112, pp. 67-96.

Comune di Sarmato (2010). Relazione Quadro Conoscitivo – Piano Strutturale Comunale.

Comune di Sarmato (2020). Relazione Illustrativa – Studio di Microzonazione Sismica Livello 2.

Doglioni C. (1993). "Some remarks on the origin of foredeeps", Tectonophysics, 228, pp. 1-20.

EC8: European Committee for Standardization (2004). Eurocode 8: design of structures for earthquake resistance. P1: General rules, seismic actions and rules for buildings. Draft 6, Doc CEN/TC250/SC8/N335.

Fantoni R., Franciosi R. (2010). "Tectono-sedimentary setting of the Po Plain and Adriatic foreland", Rend. Fis. Acc. Lincei, 21 (Suppl 1), pp. 197-209.

Foti S., Parolai S., Albarello D., *et al.* (2009). Deliverable 6: Application of surface wave methods for seismic site characterization. DPC-INGV S4 Project 2007-2009 (http://esse4.mi.ingv.it) – last accessed in June 2021 at http://esse4.mi.ingv.it/files/images/stories/deliverable_d6.pdf.

Foti S., Parolai S., Albarello D., *et al.* (2010). Deliverable 7: Application of surface wave methods for seismic site characterization of ITACA stations. DPC-INGV S4 Project 2007-2009 (http://esse4.mi.ingv.it) – last accessed in June 2021 at http://esse4.mi.ingv.it/files/images/stories/deliverable_d7.pdf.

Giustiniani M., Tinivella U., Parolai S., Donda F., Brancolini G., Volpi V. (2020). "Integrated Geophysical Analyses of Shallow-Water Seismic Imaging With Scholte Wave Inversion: The Northern Adriatic Sea Case Study", Frontiers in Earth Science, Vol. 8, p. 532 - https://www.frontiersin.org/article/10.3389/feart.2020.587898 doi:10.3389/feart.2020.587898.

Lacoss R.T., Kelly E.J. and Toksöz M.N. (1969). "Estimation of seismic noise structure using arrays", Geophysics, 34, pp. 21–38.

NTC18: Ministero delle Infrastrutture e dei Trasporti (2018). Aggiornamento delle Norme Tecniche per le Costruzioni. Part 3.2.2: Categorie di sottosuolo e condizioni topografiche, Gazzetta Ufficiale n. 42 del 20 febbraio 2018 (in Italian).

Ohori M., Nobata A. and Wakamatsu K. (2002). "A comparison of ESAC and FK methods of estimating phase velocity using arbitrarily shaped microtremor analysis", Bulletin of the Seismological Society of America, 92, pp. 2323–2332.

Okada H. (2003). The Microtremor Survey Method. SEG

Parolai S., Picozzi M., Richwalski S.M. and Milkereit C. (2005). "Joint inversion of phase velocity dispersion and H/V ratio curves from seismic noise recordings using a genetic algorithm, considering higher modes", Geophysical Research Letters, 32, L01303. doi:10.1029/2004GL021115.

Parolai S., Richwalski S.M., Milkereit C. and Fäh D. (2006). "S-wave velocity profile for earthquake engineering purposes for the Cologne area (Germany)", Bulletin of the Earthquake Research Institute, 4, pp. 65–94. doi:10.1007/s10518-005-5758-2.

PCM-DPC (1972). Italian Strong Motion Network. Presidency of Council of Ministers (PCM) - Civil Protection Department (DPC). https://doi.org/10.7914/SN/IT.

Regione Emilia Romagna – Geoportale - https://geoportale.regione.emilia-romagna.it/it.

Servizio Geologico d'Italia – Carta Geologica d'Italia scala 1:100.000 - sgi.isprambiente.it/geologia100k/mostra_foglio.aspx?numero_foglio=60.

Technical Commission SM, 2015 – Microzonazione sismica. Standard di rappresentazione e archiviazione informatica, Versione 4.0b (Commissione tecnica inter-istituzionale per la MS nominata con DPCM 21 aprile 2011).

Tokimatsu K., Tamura S. and Kojima H. (1992). "Effects of multiple modes on Rayleigh wave dispersion characteristics", Journal of Geotechnical Engineering, 118, pp. 1529–1543.

Wang R. (1999). "A simple orthonormalization method for stable and efficient computation of Green's functions", Bulletin of the Seismological Society of America, 89, pp. 733–741.

Yamanaka H. and Ishida H. (1996). "Application of generic algorithms to an inversion of surface-wave dispersion data", Bulletin of the Seismological Society of America, 86, pp. 436–444.

Disclaimer and limits of use of information

The INGV, in accordance with the Article 2 of Decree Law 381/1999, carries out seismic and volcanic monitoring of the Italian national territory, providing for the organization of integrated national seismic network and the coordination of local and regional seismic networks as described in the agreement with the Department of Civil Protection.
INGV contributes, within the limits of its skills, to the evaluation of seismic and volcanic hazard in the Country, according to the mode agreed in the ten-year program between INGV and DPC February 2, 2012 (Prot. INGV 2052 of 27/2/2012), and to the activities planned as part of the National Civil Protection System. In particular, this document[1] has informative purposes concerning the observations and the data collected from the monitoring and observational networks managed by INGV. INGV provides scientific information using the best scientific knowledge available at the time of the drafting of the documents produced; however, due to the complexity of natural phenomena in question, nothing can be blamed to INGV about the possible incompleteness and uncertainty of the reported data.
INGV is not responsible for any use, even partial, of the contents of this document by third parties and any damage caused to third parties resulting from its use. The data contained in this document is the property of the INGV.
This study has benefited from funding provided by the Italian Presidenza del Consiglio dei Ministri – Dipartimento della Protezione Civile (DPC). This paper does not necessarily represent DPC official opinion and policies.

Esclusione di responsabilità e limiti di uso delle informazioni

L'INGV, in ottemperanza a quanto disposto dall'Art. 2 del D.L. 381/1999, svolge funzioni di sorveglianza sismica e vulcanica del territorio nazionale, provvedendo all'organizzazione della rete sismica nazionale integrata e al coordinamento delle reti sismiche regionali e locali in regime di convenzione con il Dipartimento della Protezione Civile.
L'INGV concorre, nei limiti delle proprie competenze inerenti la valutazione della Pericolosità sismica e vulcanica nel territorio nazionale e secondo le modalità concordate dall'Accordo di programma decennale stipulato tra lo stesso INGV e il DPC in data 2 febbraio 2012 (Prot. INGV 2052 del 27/2/2012), alle attività previste nell'ambito del Sistema Nazionale di Protezione Civile. In particolare, questo documento[1] ha finalità informative circa le osservazioni e i dati acquisiti dalle Reti di monitoraggio e osservative gestite dall'INGV. L'INGV fornisce informazioni scientifiche utilizzando le migliori conoscenze scientifiche disponibili al momento della stesura dei documenti prodotti; tuttavia, in conseguenza della complessità dei fenomeni naturali in oggetto, nulla può essere imputato all'INGV circa l'eventuale incompletezza ed incertezza dei dati riportati.
L'INGV non è responsabile dell'utilizzo, anche parziale, dei contenuti di questo documento da parte di terzi e di eventuali danni arrecati a terzi derivanti dal suo utilizzo. La proprietà dei dati contenuti in questo documento è dell'INGV.
Lo studio presentato ha beneficiato del contributo finanziario della Presidenza del Consiglio dei Ministri – Dipartimento della Protezione Civile; la presente pubblicazione, tuttavia, non riflette necessariamente la posizione e le politiche ufficiali del Dipartimento.

[1]This document is level 3 as defined in the "Principi della politica dei dati dell'INGV (D.P. n. 200 del 26.04.2016)"